Quarterly Report: July 2010

Methane Recovery from Hydrate-bearing Sediments

Funding Number: DE-FC26-06NT42963

Submitted By:

J. Carlos Santamarina
Georgia Institute of Technology
School of Civil and Environmental Engineering
Atlanta, GA 30332-0355
Phone: (404)-894.7605
Fax: (404)-894.2278
E-mail: jcs@gatech.edu

Costas Tsouris
Oak Ridge National Laboratory
Georgia Institute of Technology
School of Civil and Environmental Engineering
Atlanta, GA 30332-0373
E-mail: costas.tsouris@ce.gatech.edu

Acknowledgment: "This material is based upon work supported by the Department of Energy under Award Number DE-FC26-06NT42963."

INTRODUCTION - ANTICIPATED MAIN RESULTS

Goals: Identifying, understanding and modeling processes involved in methane production from hydrate-bearing sediments.

Approach: observation and interpretation of phenomena at multiple scales, ranging from pore-contact scale to the macro-reservoir scale, taking into consideration various possible driving forces (e.g., depressurization, thermal stimulation).

Anticipated results and most significant contributions: In view of our experience accumulated since the beginning of the project, we anticipate that some of the main results from this study will address:

- *Hydrate formation and growth*. Different conditions (unsaturated from gas phase, from ice, from dissolved phase, in water-wet and oil-wet sediments, during gas exchange). Formation rates at gas-water interface. Transients. Spatial distribution (partial pore filling, cluster, segregated).
- *Relevance to marine and permafrost environments*.
- *Hydrate-mineral bonding and tensile strength*. Implications on the mechanical behavior of hydrate bearing sediments in view of production strategies.
- *Gas production by heating and depressurization*. Study in 5m long 1D cell. Experimental study and modeling.
- *Gas production by chemo-driven methods*. Fundamental understanding of CO_2-CH_4 exchange.
- *Gas production by transients*.
- *The role of effective stress* in formation and production.
- *Gas invasion versus gas production* – Evolution of degree of saturation and fluid conduction. Fluid-driven fractures.
- *Fluid conductivity in spatially varying sediments*
- *Thermodynamic formulation*
- *Coupled Thermo- Hydro- Chemo-Mechanical formulation*.
- *Production strategies in different formations*
- *Relevance to real systems*

Research Team: The current team is shown next.

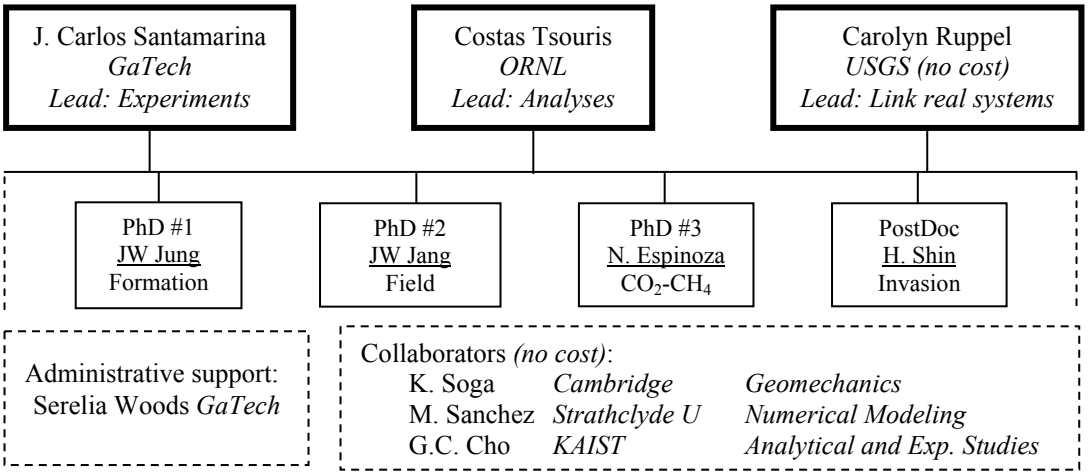

SUMMARY OF RESEARCH DEVELOPMENTS DURING THIS QUARTER

During this quarter, the research team has been dedicated to completing test sequences, advancing analyses, simulating numerical modeling and preparing manuscripts for all tasks reported in previous quarterly reports. The most relevant themes have included:

- CH_4-CO_2 replacement
  - Pore scale experiments
  - Macroscale experiments
  - Measurement of electrical resistance and mechanical impedance during CH_4-CO_2 hydrate replacement
- Micro-model fabrication for production studies
- Simulation of conductivity at different hydrate saturation and comparison with other models.
- Evolution of gas and water saturation during gas invasion and gas nucleation
- Advanced studies on hydrate lens formation – implications of lense dissociation

CH_4-CO_2 replacement – Pore Scale Study

The test consists of a thin cylindrical water layer (8.8mm diameter, 0.9mm in height; and 55mg water mass) retained by surface tension between two conductive aluminum disks (see figure – pane a). These disks are bonded onto corresponding piezocrystals. The device is housed in a high pressure chamber within a temperature controlled environment (see figure – pane b). Pane c in the figure shows the electrical circuit and peripheral electronics used to measure electrical resistance and relative stiffness. Electrical resistance is determined at an input frequency of 50*kHz* to avoid electrode polarization effects. The resistance of the medium R is a function of measured voltages V_1 and V_2, and the known resistance of the series resistor R^*=4700Ω. The source piezocrystal is connected to a signal generator that is operated at ultrasound frequencies (continuous ~60*kHz* sinusoid).

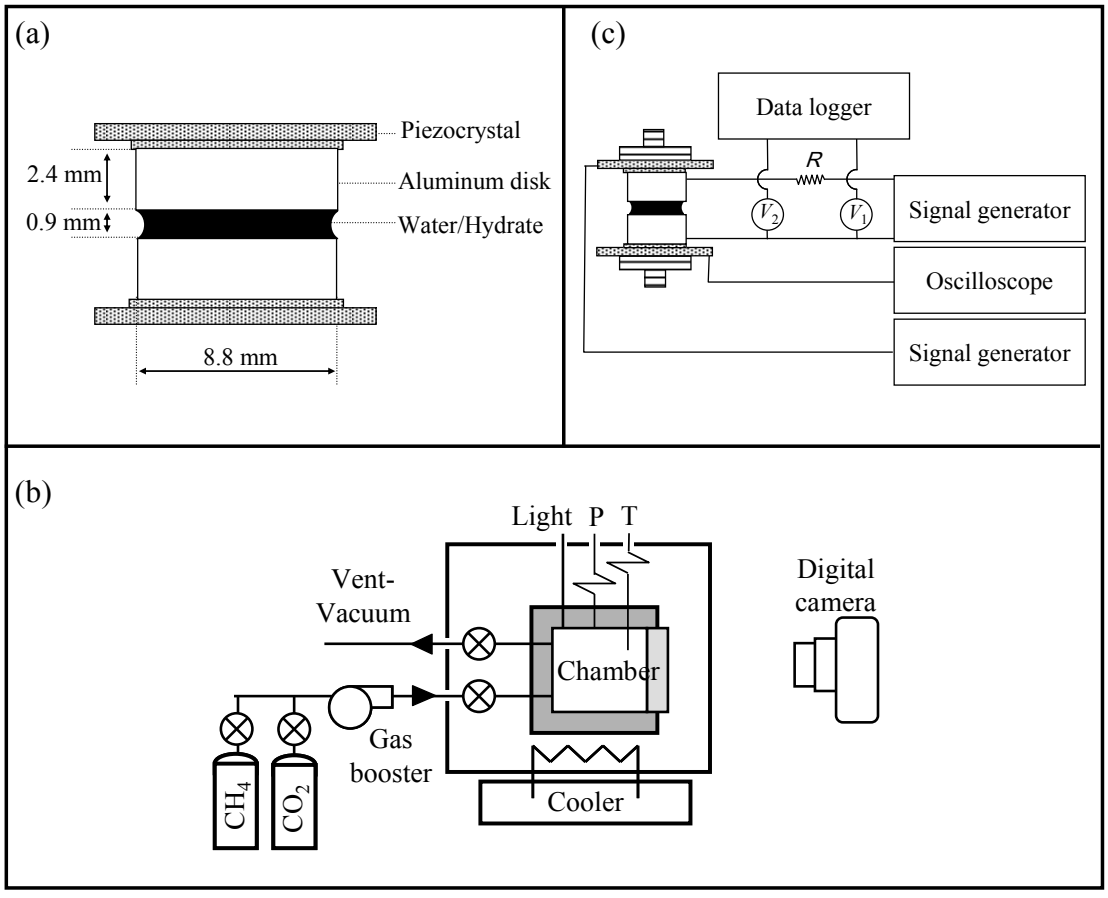

Test Procedure. The P-T trajectory during this experiment consists of three stages: (1) ice formation and melting followed by CH_4 hydrate formation, (2) CH_4-CO_2 replacement, and (3) hydrate dissociation. (a0) Water, (a1) Ice formation, (a2) Ice melts, (a3 and a4) CH_4 hydrate phase boundary, (b1) CO_2 injection; (b2) liquid CO_2 forms in the chamber, (c0) Depressurization, (c1) Gas-liquid CO_2 phase boundary, (c2) CH_4 hydrate phase boundary, (c3) CO_2 hydrate phase boundary, and (c4) End of test.

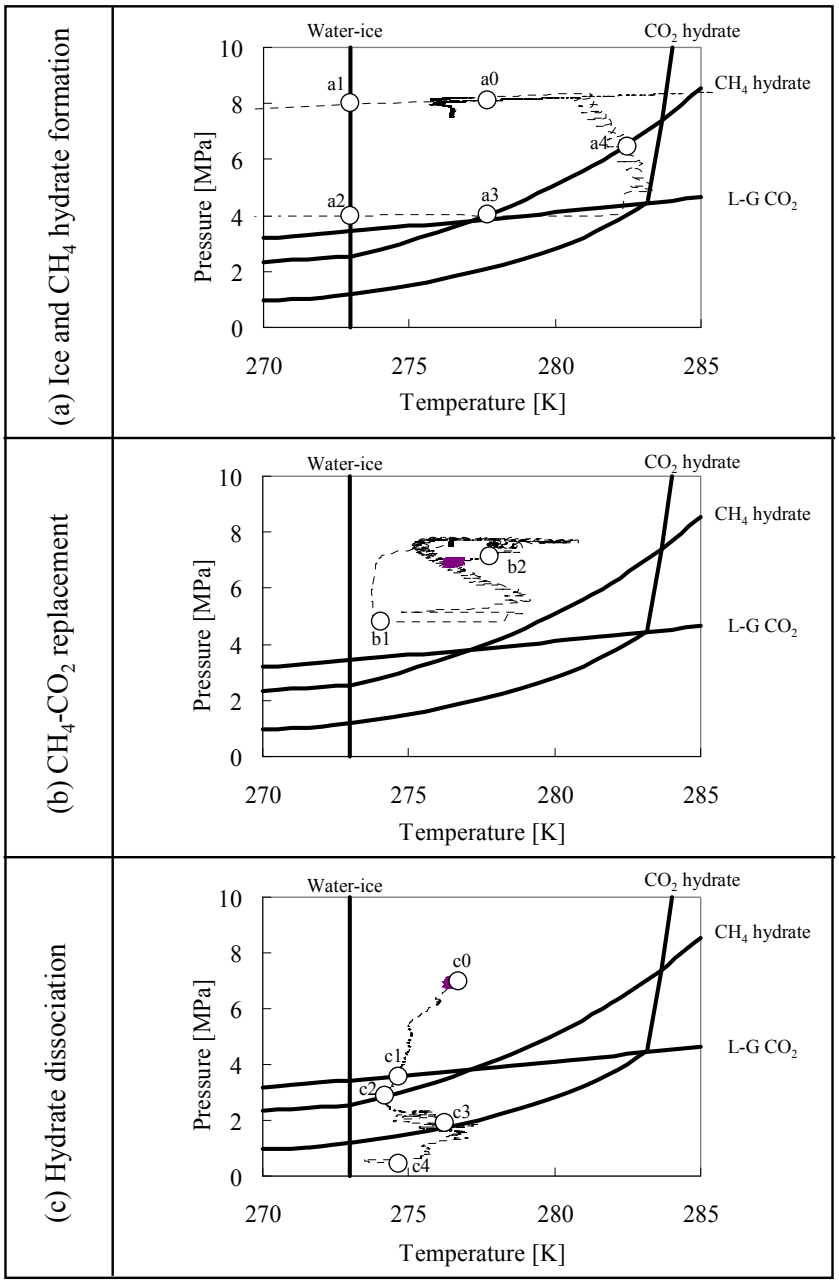

Results. The evolution of pressure, temperature, electrical resistance, and relative stiffness during the experiment is shown next. Specific events include: (a0) Water, (a1) Ice formation, (a2) Ice melts, (a3 and a4) CH_4 hydrate phase boundary, (b1) Gas CO_2 injection reaches liquid CO_2 at b2, (c0) Depressurization, (c1) CO_2 G-L phase boundary, (c2) CH_4 hydrate phase boundary, (c3) CO_2 hydrate phase boundary, and (c4) End of test.

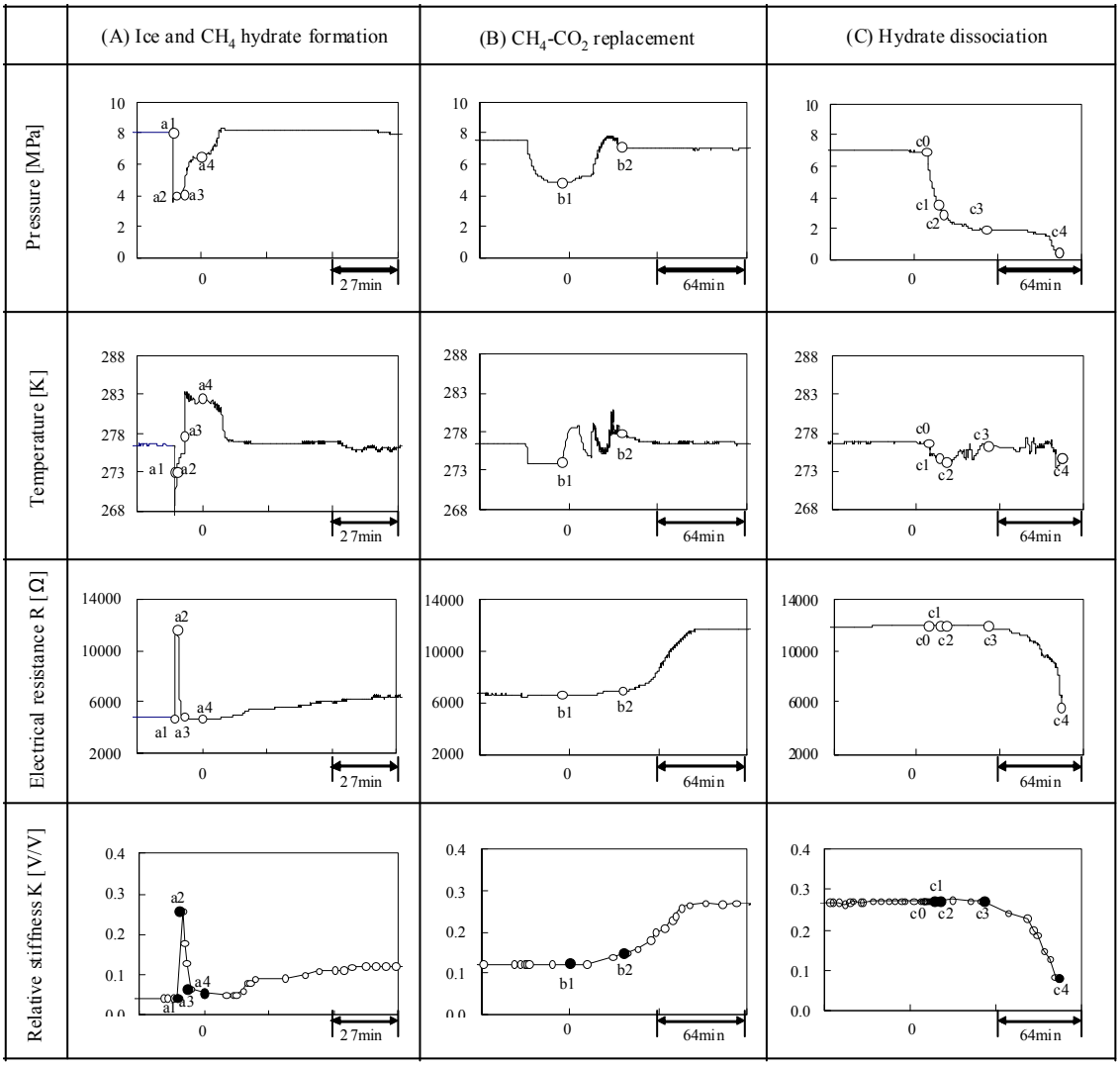

Time-Lapse Photographs. CH_4-CO_2 Replacement experiment. (a) Water droplet – Scale: 8.8mm diameter, 0.9mm length of water meniscus (b) Ice formation, (c),(d) CH_4 hydrate formation and growth, (e) Injection of liquid CO_2, (f) Hydrate growth, (g) Depressurization out of CH_4 hydrate stability field, and (h) Image after hydrate dissociation.

(a) 0min - Water [8.1MPa, 276K, Fig. 2(a0-a1)	(b) 100min - Ice [3.7MPa, 250K, Fig. 2(a1-a2)	(c) 300min – In CH_4 [8.1MPa, 276K, Fig. 2-a5	(d) 1050min – In CH_4 [8.1MPa, 276K, Fig. 2
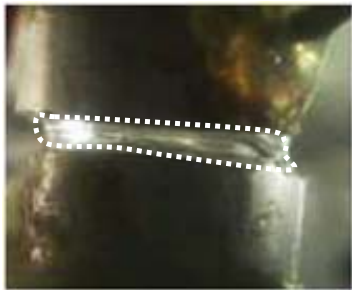	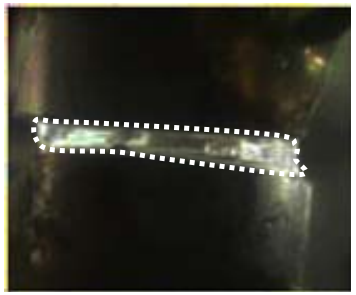	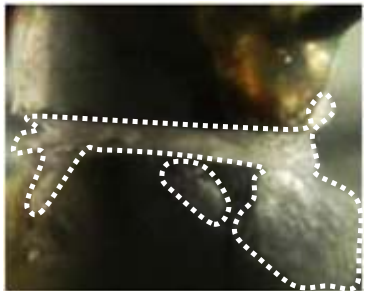	
(e) 1250min – In liquid CO_2 [7.0MPa, 276K, Fig. 2(b1-b2)	(f) 1550min – In liquid CO_2 [7MPa, 276K, Fig. 2(b1-b2)	(g) 1800min – In gas CO_2 [2.5MPa, 275K, Fig. 2(c1-c2)	(h) 2010min – In gas CO_2 [0.5MPa, 275K, Fig. 2
			

Conclusions

- Contact-scale electrical resistance and relative stiffness measurements provide unique insight into hydrate formation, CH_4-CO_2 replacement, and hydrate dissociation.
- CH_4 hydrate formation is diffusion controlled, and it is much slower than heat-transport limited ice melting (at mm-scale). Therefore, hydrate formation is not concurrent with ice melting in most laboratory and field situations.
- Both CH_4 hydrate formation and CH_4-CO_2 replacement cause volume expansion.
- Free water can remain in an excess CH_4 gas system for a long time because hydrate formation is limited by the slow diffusion of CH_4 through the hydrate shell that forms between water and gas.
- While CH_4-CO_2 replacement requires destructing of the hydrate cage (i.e, a solid-liquid-solid transformation), both electrical resistance and relative stiffness measurement show that CH_4-CO_2 replacement occurs locally and gradually so that the overall hydrate mass remains solid and no stiffness loss or changes in resistance should be expected at the sediments scale.

Experimental Micro-models

Two-dimensional micro-models facilitate the observation of phenomena happening during hydrate formation, dissociation and CH_4-CO_2 replacement. Micro-models are made of soda-lime glasses by photo-lithography and wet-etching method. We are conducting several studies using these models including gas production, evolution of gas saturation, gas pipe formation, fluid fingering, and CH_4-CO_2 replacement. Device and preliminary experimental results follow.

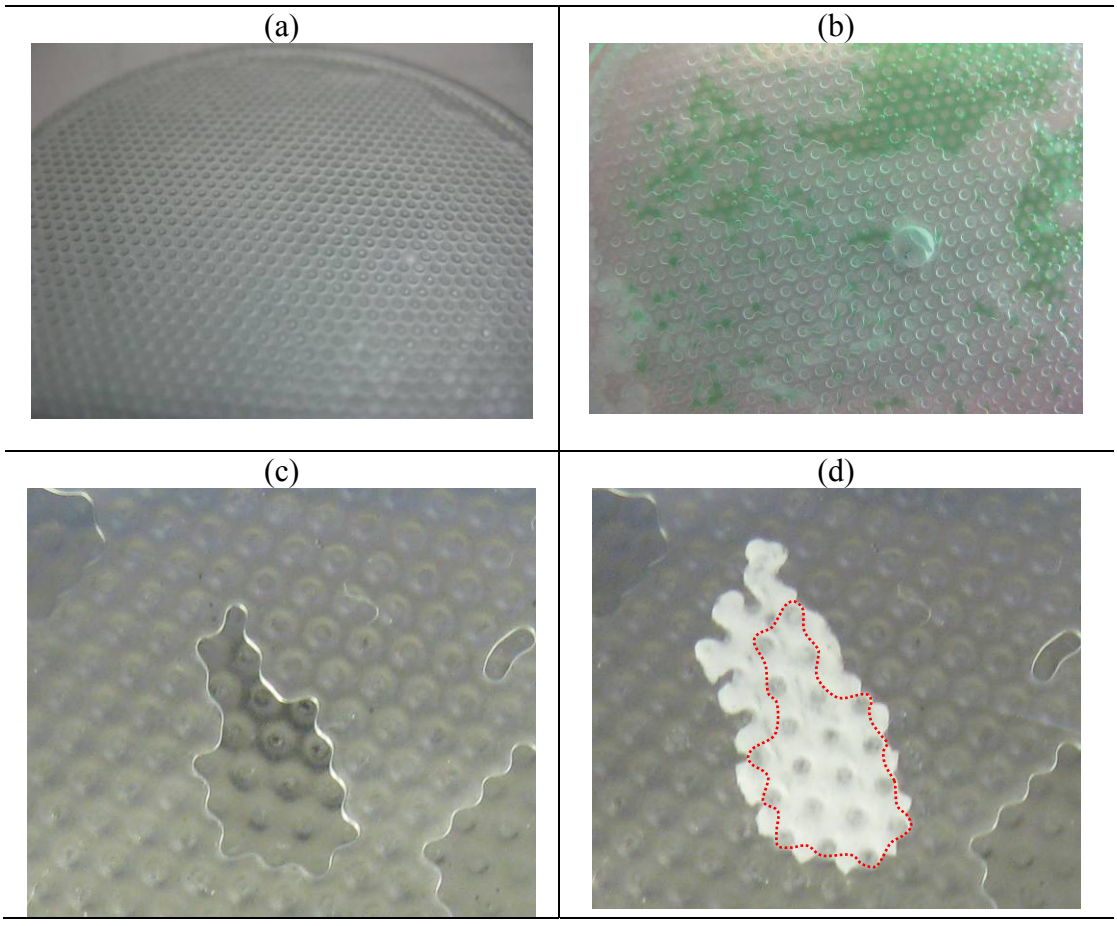

(a) Micro-model after glass-etching. (b) Green-dyed water at meniscus. (c) Water cluster. (d) Ice cluster. Substantial sub-cooling and high gas pressure above hydrate phase boundary are needed to make CH_4 and CO_2 hydrates form. Sub-cooling does not make all water clusters convert into ice.

Numerical Network Models – Recent Studies

Tube- and pore-network model have been developed and used to explore the several phenomena such as gas invasion, gas nucleation, and gas production from hydrate bearing sediment.

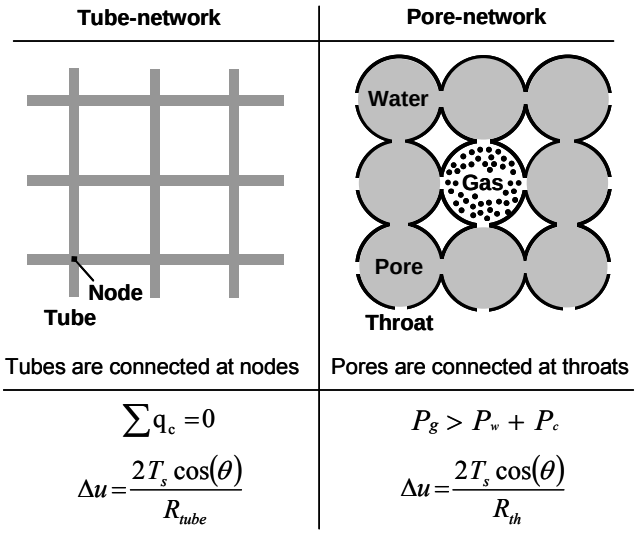

Several algorithms during gas invasion and gas nucleation are considered. The trapping algorithm (tight trapping vs. loose trapping) shows whether the defending phase (whose both ends are invaded) can be displaced. Piston-type displacement is adopted in this study.

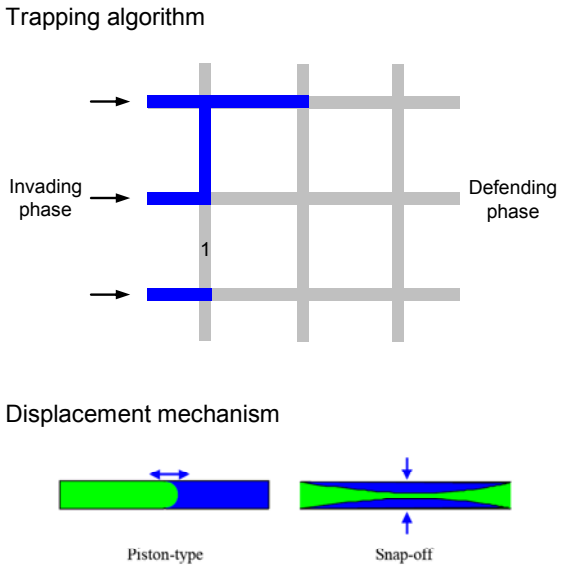

Study of Conductivity. A three-dimensional tube-network model is used to simulate water conductivity of different for different degrees of hydrate saturation and hydrate distribution habit. Models under consideration include:

■ Capillary tube model

$k_{rw} = (1 - S_h)^2 = S_w^2$ forming by coating

$k_{rw} = 1 - S_h^2 + \frac{2(1 - S_h)^2}{\log(S_h)} = 1 - (1 - S_w)^2 + \frac{2S_w^2}{\log(1 - S_w)}$ forming from center

■ Kozeny model

$k_{rw} = (1 - S_h)^{n+1} = S_w^{n+1}$ forming by coating n=1.5 ($0<S_h<0.8$) [Spangenberg, 2001]

$k_{rw} = \frac{(1 - S_h)^{n+2}}{(1 + S_h^{0.5})^2} = \frac{S_w^{n+2}}{(1 + (1 - S_w)^{0.5})^2}$ forming by center n=0.4~1 ($0.1<S_h<1$) [Spangenberg, 2001]

■ University of Tokyo model

$k_{rw} = (1 - S_h)^N = S_w^N$

N=2 Hydrate coating
N=2~15 [Scheidegger, 1960; Masuda et al., 1997]
N=2.6 [MInagawa et al., 2004]
N=9.8 [MInagawa et al., 2004]
$N=10.384S_h^2-27.773S_h+13.639$ ($0<S_h<0.3$) [Sakamoto et al., 2008]

■ University of Tokyo model

$k_{rw} = S_w^{1/2}\left[1 - (1 - S_w^{1/m})^m\right]^2 \quad S_w = \frac{S_w' - S_r}{1 - S_r}$ [van Genuchten, 1980; Moridis et al., 2008]

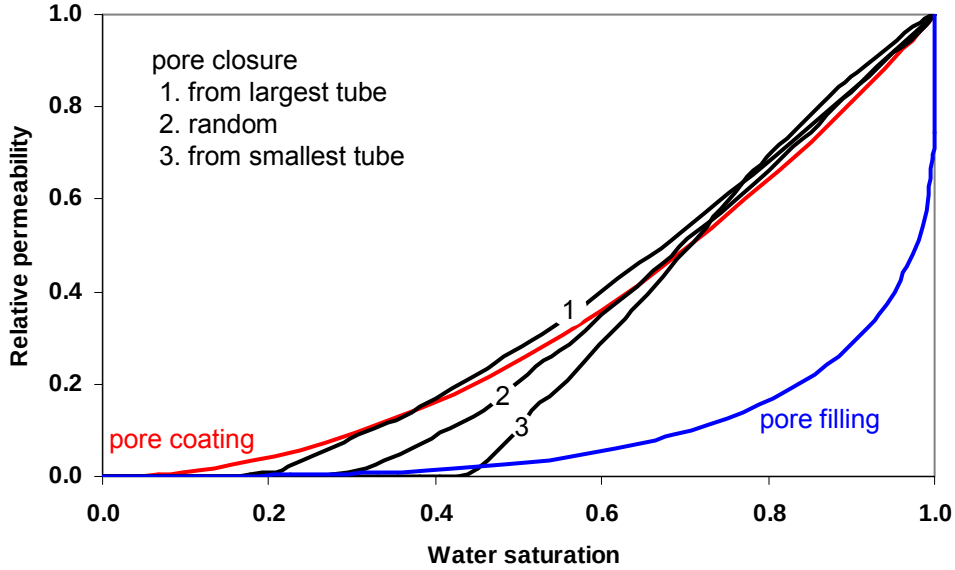

Relative permeability as a function of hydrate saturation. It is assumed that hydrates form by (1) coating pore, (2) filling pore, and (3) closing pore one-by-one. Three-dimensional tube network model is used; 13×13×13 nodes, 3575 tubes, $\sigma(\ln(R/[\mu m])=0.4$.

Study of factors that control characteristics curves (P_c-S relation). Water retention and capillary pressure are affected by several parameters. Capillary pressure is a function of surface tension, contact angle, and pore throat radius.

$$P_c = \frac{2T_s \cos(\theta)}{R_{th}} \qquad \text{Capillary pressure}$$

A tube-network model is used to study the effect of these parameters on the characteristic curves. Results confirm that the capillary pressure generally increases as (a) contact angle decreases, (b) surface tension decreases, and (c) mean tube size increases. As the coefficient of variation in tube size increases, there are more small tubes and extremely large tubes occur; the effect is shown in pane-d (Note the different residual saturation at different COV values)

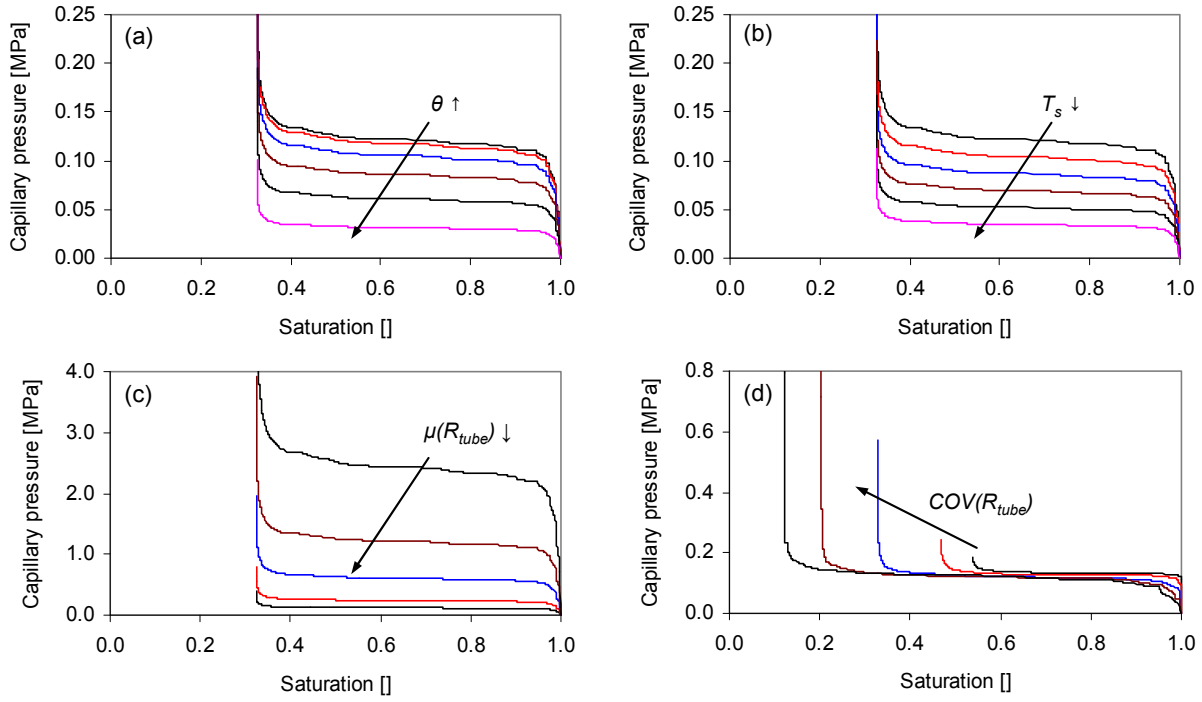

Parameters that affect the characteristic curve (the relation of P_c to saturation). (a) Effect of contact angle. Used contact angle: 0, 15, 30, 45, 60, and 75°. (b) Effect of surface tension. Used surface tension: 0.07, 0.06, 0.05, 0.04, 0.03, and 0.02N/m. (c) Effect of mean tube size. Used mean tube size: 1, 0.5, 0.2, 0.1, and 0.05μm. (d) Effect of coefficient of variation in tube radius COV(R_{tube}). Mean tube size increases with increasing COV(R_{tube}). Three-dimensional tube network model is used; 13×13×13 nodes, 3575 tubes.

Study of gas saturation and relative permeability during gas invasion and nucleation. The characteristic curves for spatially uncorrelated random-distributed pores are shown. Results are almost identical for gas invasion and gas nucleation. Gas and water conductivity during gas invasion and nucleation are calculated at different saturation. Computed water conductivities are normalized by the water conductivity of the fully water saturated network. Gas conductivities are normalized by the gas conductivity obtained when gas invasion process is completed. The normalized water conductivities are almost the same for both gas invasion and nucleation. However, gas conductivity during nucleation is much lower than during gas invasion (Note: Similar conclusions were reached by Poulsen et al. (2001) using different model characteristics)

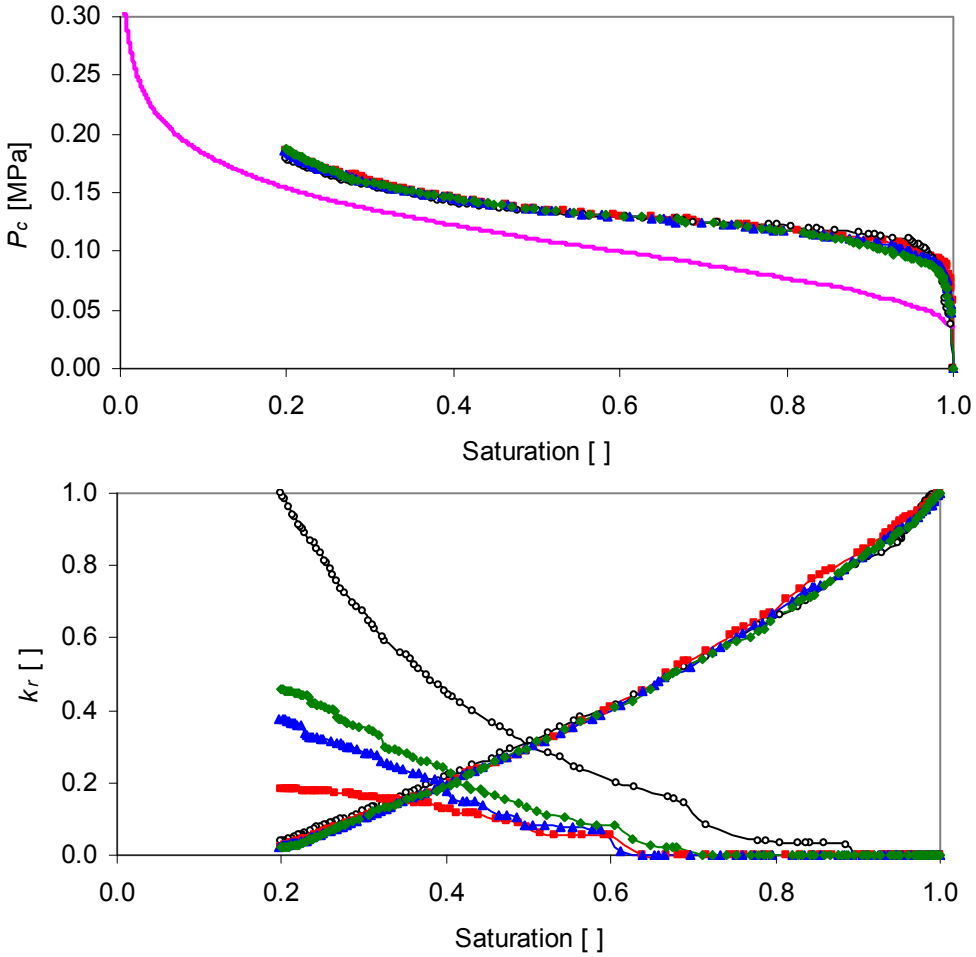

Characteristic curves and relative permeabilities - Gas invasion vs. gas nucleation. (a) Characteristic curves. Symbols: (○) gas invasion through 13^2 nodes on one side, (-) gas invasion into the network sorted by tube size; gas invasion through multiple nodes distributed inside network model: (□) 13^2, (Δ) 2×13^2, (◊) 3×13^2 nodes. (b) Relative conductivity of water k_{rw} and gas k_{rg}. Results obtained using a three dimensional tube-network model. Details: 13×13×13 nodes, 5460 tubes, coordination number cn=6, log-normal distribution of tube radius R, the mean tube size μ(R)=1μm, and the standard deviation in tube radius σ(ln(R/[μm]))=0.4.

Hydrate lens formation

The study of lense formation continues, in view of production strategies from segregated hydrates in fine-grained sediemnts. The hydrate lens thickness is calculated by methane concentration, solubility, and porosity before and after hydrate formation.

$$\frac{t}{L} = \frac{c_0 - c_f}{c_h - c_f} n_0$$ Hydrate lens thickness

Preliminary calculations show that the thickness of hydrate lens can be t=3mm for lenses separated every L=10cm of sediment (n_0=0.4, c_0=0.65mol/L, c_f=0.07mol/L, and c_h=7.69mol/L).

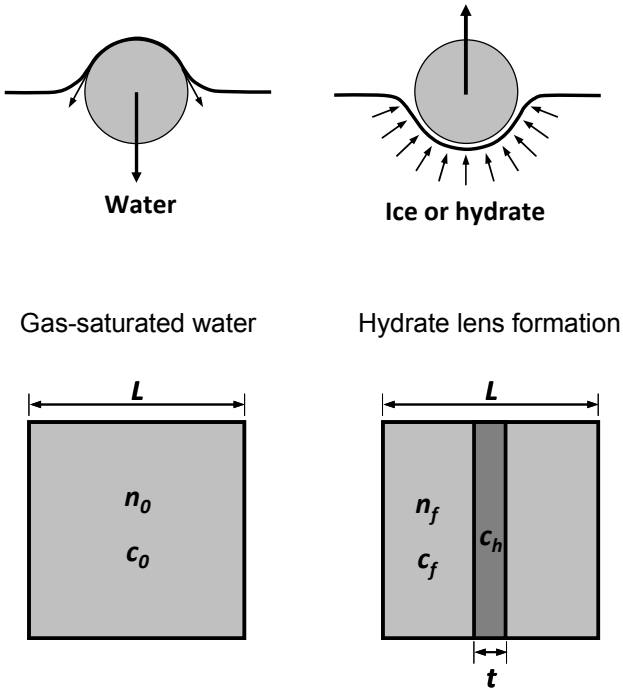

$$n_0 c_0 L = n_f c_f (L - t) + c_h t \quad \Rightarrow \quad \frac{t}{L} = \frac{c_0 - c_f}{c_h - c_f} n_0$$

$$n_f = \frac{L n_0 - t}{L - t}$$